

Community Graph Convolution Neural Network for Alzheimer's Disease Classification and Pathogenetic Factors Identification

Xia-An Bi¹, *Member, IEEE*, Ke Chen, Siyu Jiang, Sheng Luo, Wenyan Zhou, Zhaoxu Xing, Luyun Xu, Zhengliang Liu², and Tianming Liu³, *Senior Member, IEEE*

Abstract—As a complex neural network system, the brain regions and genes collaborate to effectively store and transmit information. We abstract the collaboration correlations as the brain region gene community network (BG-CN) and present a new deep learning approach, such as the community graph convolutional neural network (Com-GCN), for investigating the transmission of information within and between communities. The results can be used for diagnosing and extracting causal factors for Alzheimer's disease (AD). First, an affinity aggregation model for BG-CN is developed to describe intercommunity and intracommunity information transmission. Second, we design the Com-GCN architecture with intercommunity convolution and intracommunity convolution operations based on the affinity aggregation model. Through sufficient experimental validation on the AD neuroimaging initiative (ADNI) dataset, the design of Com-GCN matches the physiological mechanism better and improves the interpretability and classification performance. Furthermore, Com-GCN can identify lesioned brain regions and disease-causing genes, which may assist precision medicine and drug design in AD and serve as a valuable reference for other neurological disorders.

Index Terms—Alzheimer's disease (AD), community graph convolution (Com-GC) neural network, deep learning, imaging genomics.

Manuscript received 12 December 2022; revised 21 March 2023; accepted 19 April 2023. This work was supported in part by the National Natural Science Foundation of China under Grant 62072173; in part by the Hunan Provincial Innovation Foundation for Postgraduate under Grant CX20210504; in part by the Key Open Project of Key Laboratory of Data Science and Intelligence Education (Hainan Normal University), Ministry of Education, under Grant DSIE202101; in part by the National Key Research and Development Program of China under Grant 2020YFB2104400; in part by the Medical Humanities and Social Sciences Project of Hunan Normal University; and in part by the Innovation and Entrepreneurship Training Program of Hunan Xiangjiang Artificial Intelligence Academy. (*Corresponding authors: Xia-An Bi; Luyun Xu; Tianming Liu.*)

Xia-An Bi, Ke Chen, Siyu Jiang, Sheng Luo, Wenyan Zhou, and Zhaoxu Xing are with the College of Information Science and Engineering and the Key Laboratory of Computing and Stochastic Mathematics (Ministry of Education), School of Mathematics and Statistics, Hunan Normal University, Changsha, Hunan 410081, China (e-mail: bixiaan@hnu.edu.cn).

Luyun Xu is with the College of Business, Hunan Normal University, Changsha 410081, China (e-mail: xuluyun@hunnu.edu.cn).

Zhengliang Liu and Tianming Liu are with the Department of Computer Science and Bioimaging Research Center, The University of Georgia, Athens, GA 30602 USA (e-mail: tliu@uga.edu).

Color versions of one or more figures in this article are available at <https://doi.org/10.1109/TNNLS.2023.3269446>.

Digital Object Identifier 10.1109/TNNLS.2023.3269446

2162-237X © 2023 IEEE. Personal use is permitted, but republication/redistribution requires IEEE permission. See <https://www.ieee.org/publications/rights/index.html> for more information.

I. INTRODUCTION

THE prevalence of Alzheimer's disease (AD) is on a steep rise, making it the most pervasive neurodegenerative disorder and a significant cause for concern. The disease manifests as brain dysfunction, leading to problems such as slow reactions, slurred speech, unpredictable emotions, uncontrolled behaviors, and even death [1]. Because the current clinical diagnosis of AD overwhelmingly relies on detailed clinical disease histories of patients, time-consuming diagnostic procedures, and experienced neurologists, designing and developing efficient computer-aided tools is, however, highly desired for accurate AD assessment.

Up until now, attempts to treat AD have yielded limited results because of the limited acquaintance with the underlying mechanism of the formation and abnormalities of brain function. To investigate this brain disease, many researchers have used neural images, such as diffusion tensor imaging (DTI), structural magnetic resonance imaging (sMRI) and functional magnetic resonance imaging (fMRI), etc., to construct brain networks [2], [3]. Although these efforts substantiated that brain functions are inextricably linked to the collaboration between brain regions, the role of genes in regulating brain regions seems to have been overlooked. Therefore, it is more suitable to construct a more complex, large-scale network system based on the association between brain regions and genes than just based on brain regions [4]. Moreover, in actual physiological activities, functionally connected brain regions and genes collaborate in groups. "Community" is a property describing the association of structure in complex networks, which can well describe such a characteristic. With connections between brain regions and genes in a community resembling ordinary highways and connections between different communities resembling freeways, network systems can efficiently perform information storage and transmission in the brain. Community-based networks, however, have not been studied in the field of formation and abnormal mechanisms of brain function.

During the development of AD, abnormalities in intraneuronal signaling or mediated transmission of genes in the brain occur, which, in turn, leads to impairment of brain functions in behavior, language, memory, and other clinical manifestations [5]. Most existing studies have discussed the

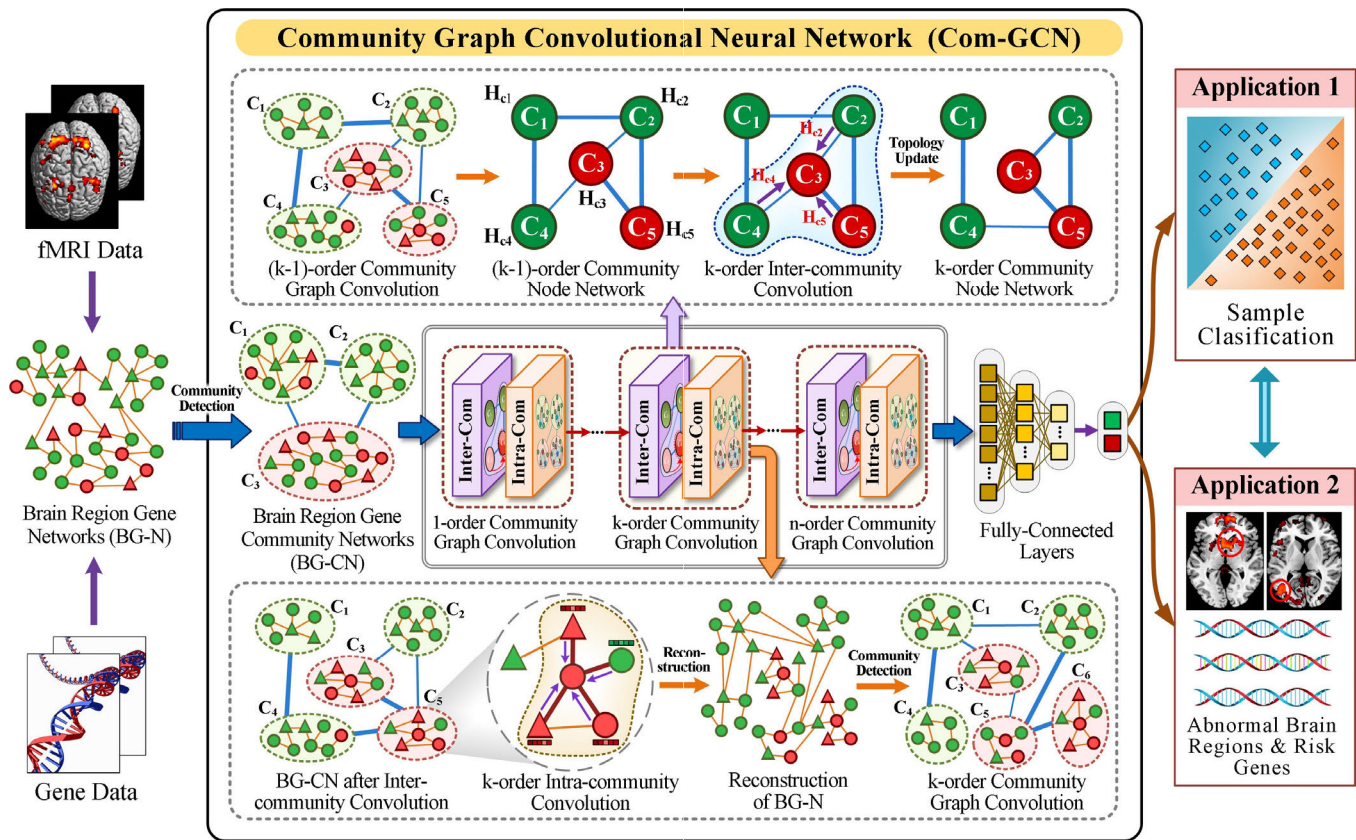


Fig. 1. Flowchart of the proposed Com-GCN. First, the BG-CN's are constructed. Second, the Com-GCN is established using the affinity aggregation model. Finally, the Com-GCN can finish the tasks of subject classification and characteristic extraction.

relationship between them using trivial networks to explore the process of disease formation. Nevertheless, disease-induced dysfunction can be divided into two aspects. First, at the community level, lesions in brain regions or mutations in risk genes can affect closely connected brain regions or genes, which will lead to a reduction in the efficiency of local information interaction and can be reflected as abnormalities in the internal structure of the community. Second, on a larger scale, abnormal brain regions or genes can lead to a reduction in the efficiency of intercommunity information interaction, which is reflected as an abnormality in the intercommunity correlations. Theoretically, by analyzing the structural differences of communities, we can pinpoint the disease state of the patients [6], [7]. Therefore, it is reasonable and necessary to introduce the community structure to study brain diseases.

The community structure contains important information that reflects the structure and function of the network and also profoundly affects the mode of information dissemination within the network, which has been validated in the fields of nature, engineering, society, and economy [8], [9]. Therefore, the analysis of community structure in complex networks is an attractive topic, and some valuable research results have been achieved [10]. In community structure-based studies, statistical methods are applied to key node identification [11], traditional machine learning methods are usually used for link prediction [12], and deep learning methods combined with community analysis are used for advanced link

predictions [13]. The study of community structure based on community detection helps reveal the organizational mechanisms of complex systems. The study of AD classification, however, has not used many existing algorithms that incorporate community structures.

In this article, through the integration of complex network theory and deep learning, we explore the construction of brain region gene community networks (BG-CN's) and the differences between community structures. We then propose the community graph convolutional neural network (Com-GCN) for AD diagnosis. The overall framework of Com-GCN is shown in Fig. 1.

First, the initial BG-CN was constructed by community detection on the brain region gene network (BG-N) constructed from brain imaging data and gene data of subjects. Second, the clustering of brain regions and genes in communities and the functional collaboration between different communities are modeled as the process of community detection and information interaction. Accordingly, the affinity aggregation model is proposed. Third, Com-GCN, including the community graph convolution (Com-GC) layers, is designed. Each Com-GC layer contains interconvolution and intraconvolution operations. In particular, the interconvolution operation makes every community aggregate the information of neighboring communities and updates the intercommunity correlation structure. As a result of the intraconvolution operation, every node within a community aggregates the characteristic information

of neighboring nodes, thereby updating the topology of BG-N. Finally, after n times of Com-GC, based on the updated BG-N, more precise community detection can be performed to obtain a more authentic BG-CN, based on which the Com-GCN can output classification results for each subject and further identify the AD-related genes and brain region lesions. Our contributions are summarized below.

1) The BG-CN is constructed for each subject, and brain imaging data and genetic data are fused from a community perspective to describe higher order associations between brain regions and genes.

2) The proposed Com-GCN combines deep learning with the community structure to acquire high interpretability, which is the first time that the community concept is applied to AD diagnosis research. It can extract the salient regions that facilitate classification during the training process, accurately diagnose whether one suffers from AD, and further find the specific lesion brain regions and pathogenic genes.

3) Our experiments using the AD neuroimaging initiative (ADNI) dataset have demonstrated that Com-GCN surpasses cutting-edge techniques for classification in all instances.

The article is structured as follows. After the introduction, Section II provides a review of previous research focused on community structure application and AD classification. Then, we present the proposed methodology in detail with the derivation of equations in Section III. The study data, competition methods, experimental setup, and experimental results are introduced in Section IV. Section V of the article offers a comprehensive examination of our effectiveness of approach while also highlighting any current limitations and presenting potential future research directions. Finally, in Section VI, we had a conclusion.

II. RELATED WORKS

A brief review of the most relevant studies, including applied techniques based on community structure and AD classification techniques, is presented in the following paragraphs.

A. Community Structure-Based Research

As a prevalent and essential topological feature of information dissemination in complex networks, community structure has received close attention in different fields. In networks, key nodes refer to those nodes that play a crucial role in information propagation. Research on key node identification based on community structures has obtained considerable achievements. In biological networks, the proteins, metabolites, or genes with significant biological or pathological significance are frequently identified as the key nodes. Rivalta and Batista [14] developed the community network analysis method for analyzing protein movement at node and community levels, and the CAN method was able to identify critical proteins more efficiently. Because the community structure is characterized by dense internal connections and sparse external connections, the community structure is also applied for link prediction. Saltalamacchia et al. [15] revealed the information exchange pathways of gene-regulated spliceosomes in eukaryotes through community network analysis. These studies

indicate the significant role of community structure in the analysis of biological networks.

In AD studies, researchers extract community structure features in the brain network in order to understand the mechanism of brain dysfunction in AD patients [16]. According to Contreras et al. [17], AD patients displayed fewer larger communities and fewer connections among communities in comparison with healthy individuals. Based on 33 community detection algorithms, Dimitriadis et al. [18] tested the reproducibility of each algorithm and ultimately provided a reproducible framework for community detection in the brain structural network. Ting et al. [19] proposed a dynamic community tracking method to identify state-related changes in the organization of brain communities and discovered that the pattern of community connections under different states was more pronounced in a motor task than in a language task.

These studies demonstrate that the investigation of community structure contributes to revealing and understanding the correlation and functions of brain regions and may thus facilitate AD detection. Most previous researches were, however, conducted with traditional statistical methods for classification or feature extraction, which is inefficient and insufficiently interpretable.

B. Diagnostic Techniques for AD

More recently, numerous efforts have been made to develop computer-aided diagnostic models for AD classification. Previous approaches have shown that making full use of complementary information between different modalities can improve diagnostic accuracy [20], [21]. Conventionally, data fusion is performed by correlation analysis; for instance, as a result of the sparse canonical correlation analysis (CCA) approach, Hao et al. [22] found discriminative features in AD patients based on single nucleotide polymorphism (SNP) and sMRI data. The experimental results demonstrate the feasibility and superiority of imaging genetic data in multimodal analysis, but these methods reveal little about the specific patterns of relationships between causative factors. In traditional research, clinical experiments verify associations, while computer and data science detect correlations through coding two sequences. Researchers have achieved results in verifying the feasibility of this approach, and further exploration is possible.

Imaging data and genetic data have both been the subject of numerous machine learning methods [23], [24], [25], [26], among which the most popular method is the support vector machine (SVM). Despite its widespread use, SVM requires expert knowledge to preselect the features from the original data before training. Because of the fact that brain diseases are associated with highly dispersed and sophisticated anatomical and functional disorders, deep learning approaches are particularly suitable for the exploration of brain diseases. Gradually, some deep learning methods like deep neural networks (DNNs) convolutional neural networks (CNNs) have been proposed, as Basheera and Ram [27] proposed a novel CNN-based method for accurately detecting AD from magnetic resonance imaging (MRI). The analysis of graphs based on CNN provides a broad prospect for understanding the

organization of brain networks, and graph convolutional networks (GCNs) are one of the most representative types of CNNs particularly suitable for learning characteristics from graph data [28], [29], [30]. Zhu et al. [31] proposed a GCN-based technique for early AD diagnosis combining interpretable features with dynamic graph learning, and the results showed that correlation through graph structure could provide more accurate diagnoses.

Despite the good performance of the above methods for diagnosing AD, they are typically designed with insufficient interpretability by relying only on quantitative analysis methods of trivial networks. To address this issue, we developed the Com-GCN method, which efficiently uses the community structure information contained in the network. More information is extracted from the community structure, which provides high levels of accuracy in AD diagnosis and the ability to extract distinguishing features.

III. PROPOSED METHODS

A. Construction of BG-CN

BG-CN is constructed from BG-N by community detection. The BG-N is constructed as in our previous study. BG-N includes nodes representing brain regions and genes, edges describing the associations between nodes, and Pearson's correlation (PC) coefficient between nodes as the weights of edges, which are calculated as follows:

$$W_{ij} = \frac{l \sum f_i^k f_j^k - \sum f_i^k \sum f_j^k}{\sqrt{l \sum (f_i^k)^2 - (\sum f_i^k)^2} \sqrt{L \sum (f_j^k)^2 - (\sum f_j^k)^2}} \quad (1)$$

where l represents the length of the time sequence of one brain region or the coding sequence of one gene; f_i^k and f_j^k represent the k th feature sequences of nodes i and j , respectively.

For M subjects, M BG-CN's can be obtained, and communities can be further detected based on the centrality of nodes and the association strength of edges to create M BG-CN's. Association strength between nodes refers to the degree of internode correlation, while the centrality of nodes refers to the node centrality in the network. High node centrality indicates the node is important and closely connected with other nodes. The centrality of node i is defined as Cen_i , which can be calculated as follows:

$$\text{Cen}_i = \frac{d_i}{N-1} \quad (2)$$

where the value of i is between 1 and the total number of nodes N , and d_i represents the degree of node i .

A community can be viewed as a subnetwork with a central node being the node with the highest centrality, and the other nodes within the community should be closely connected to the central node. The modularity index Q is commonly used to measure the quality of community detection [32]. By maximizing the modularity Q to an interval between 0.3 and 0.7, the optimal network community division can

be achieved. The modularity Q is defined as follows:

$$Q = \frac{1}{2e} \sum_{i,j} \left(A_{ij} - \frac{d_i * d_j}{2e} \right) \delta(C_i, C_j) \quad (3)$$

$$A_{ij} = \begin{cases} 1, & \text{nodes } i \text{ and } j \text{ have an edge} \\ 0, & \text{nodes } i \text{ and } j \text{ have no edge} \end{cases} \quad (4)$$

$$\delta(C_i, C_j) = \begin{cases} 1, & C_i = C_j \\ 0, & C_i \neq C_j \end{cases} \quad (5)$$

where e denotes the number of network edges; \mathbf{A} represents the adjacency matrix of the network; C_i and C_j denote the community to which nodes i and j belong, respectively.

It is important to note that the modularity index Q , also known as the global modularity index, is used to measure the results of community detection on the basis of the overall network structure of the community after the completion of the network division [33]. In contrast, the local modularity index Q_l can provide an evaluation of the stability of community detection based on local community structure. Q_l is defined as follows:

$$Q_l = \frac{e_{\text{in}}}{e_{\text{in}} + e_{\text{out}}} \quad (6)$$

where e_{in} and e_{out} denote the number of edges inside and outside the community, respectively.

In general, a community with more internal edges and fewer external edges will get a higher Q_l value, indicating a clearer structure. In summary, the steps of community detection for a BG-N are as follows. To begin, rank the nodes within the network based on their centrality, and the node with the greatest centrality is the central node of the first community. Second, find the node v closest to this community among the remaining nodes, and calculate the local modularity increment ΔQ_l that will be brought to the community after v is merged with the community. When $\Delta Q_l > 0$, it means that node v can make the community structure more stable, so node v will be merged into the community; otherwise, continue to check the next nearest neighbor node. Third, repeat the second step to find and add nodes until the addition of a node causes $\Delta Q_l \leq 0$, at which time the detection of a community is completed. Last, among the remaining nodes, the node with the greatest node centrality will serve as the central node for the next community, and the above process of community detection is repeated until all nodes in the BG-N are divided into communities.

B. Affinity Aggregation Model

Collaboration between multiple brain regions and genes with similar feature information is common in achieving complex physiological activities, often leading to their classification into the same community. Interactions between communities play a crucial role in the development of physiological activities and diseases. In the evolution of BG-N, communities initially interact with each other, regulating the physiological states and behavioral activities of individuals. This is followed by changes in node information, affecting interactions within a community. To gain deeper insights into how feature

information is transmitted within and between communities, the association between nodes within a community is termed “internode affinity,” while the association between communities is known as “intercommunity affinity.” The affinity aggregation model comprises the following components.

1) *BG-CNs for Subjects*: $\mathbf{G} = \{\mathbf{G}_i | i = 1, 2, \dots, M\}$, \mathbf{G} denotes the BG-CNs constructed for M subjects.

2) *Weight of Edges*: $\mathbf{W} = \{W_{ij} | i, j = 1, 2, \dots, N\}$, a larger weight indicates a closer relationship between two nodes.

3) *Information of Communities*: $\mathbf{Hc}^{(t)} = \{\mathbf{Hc}_p^{(t)} | p = 1, 2, \dots, u\}$, the notation $\mathbf{Hc}_p^{(t)}$ denotes the information of the p th community after t th affinity aggregation, obtained by calculating the global efficiency of community p :

$$\mathbf{Hc}_p^{(t)} = \frac{1}{Nc_p(Nc_p - 1)} \sum_{i \neq j, i, j \in C_p} \frac{1}{\text{dis}_{ij}} \quad (7)$$

where Nc_p and dis_{ij} denote how many nodes are within community p and the shortest path from node i to node j within the community, respectively.

4) *Information of Nodes*: $\mathbf{H}^{(t)} = \{\mathbf{H}_i^{(t)} | i = 1, 2, \dots, N\}$, the superscript t indicates the matrix after the t th affinity aggregation, so the initial feature information matrix is $\mathbf{H}^{(0)}$.

5) *Intercommunity Affinity*: $\mathbf{Rc} = \{\mathbf{Rc}_{pq} | p, q = 1, 2, \dots, u\}$, \mathbf{Rc}_{pq} denotes the affinity between community p and community q . The greater the affinity, the closer the relationship between the communities. Nodes within two closely matched communities will have a relatively high similarity. The average similarity between the nodes of the two communities is calculated as

$$\text{Avg}(C_p, C_q) = \frac{\sum_{i \in C_p, j \in C_q} W_{ij}}{Nc_p + Nc_q}. \quad (8)$$

Then, the intercommunity affinity \mathbf{Rc}_{pq} is defined as

$$\mathbf{Rc}_{pq} = \left(\frac{\text{Avg}(C_p, C_q)}{\text{Avg}(C_p, C_p)} + \frac{\text{Avg}(C_p, C_q)}{\text{Avg}(C_q, C_q)} \right) / 2 \quad (9)$$

where Nc_p and Nc_q denote the number of nodes in the communities C_p and C_q , respectively.

6) *Internode Affinity*: $\mathbf{Rn} = \{\mathbf{Rn}_{ij} | i, j = 1, 2, \dots, N\}$, \mathbf{Rn}_{ij} denotes the internode affinity between nodes i and j , which is calculated by their common neighbors. Nodes with higher affinity will have a closer internode relationship, which will also indicate a greater information transmission efficiency between these two nodes. The formula for calculating internode affinity is as follows:

$$\mathbf{Rn}_{ij} = \sum_{k \in \Gamma_i \cap \Gamma_j} \frac{1}{\log d_k} \quad (10)$$

where Γ_i denotes the neighbors of node i , $\Gamma_i \cap \Gamma_j$ denotes the set of common neighbors between nodes i and j , and d_k denotes the degree of node k .

Based on the above components, an affinity aggregation model of the BG-CN is established, which is described by

the following equation:

$$\Delta Hc^{(k)} = \left\{ \Delta Hc_p^{(k)} = \alpha \sum_{q=1}^u \mathbf{Rc}_{pq}^{(k-1)} * Hc_q^{(k-1)} \right\} \quad (11)$$

$$\mathbf{Rc}_t^{(k)} = \left\{ \mathbf{Rc}_{pq}^{(k)} = \frac{\mathbf{Rc}_{pq}^{(k-1)}}{\sum_{k=1}^u \mathbf{Rc}_{pk}^{(k-1)}} \Delta Hc_p^{(k)} + \frac{\mathbf{Rc}_{qp}^{(k-1)}}{\sum_{k=1}^u \mathbf{Rc}_{qk}^{(k-1)}} \Delta Hc_q^{(k)} \right\} \quad (12)$$

$$\mathbf{H}^{(k)} = \left\{ \mathbf{H}_i^{(k)} = \beta \left(\sum_{j=1}^N W_{ij}^{(k-1)} * \mathbf{Rn}_{ij}^{(k-1)} * \mathbf{H}_j^{(k-1)} \right) \right\} \quad (13)$$

$$\mathbf{G}^{(k)} = \text{Community_Detection}(\mathbf{Rc}_t^{(k)}, \mathbf{H}^{(k)}) \quad (14)$$

$$\mathbf{Z}^{(n)} = \left\{ \mathbf{Z}_i^{(n)} = \frac{e_{p_i} - \bar{e}_p}{\sigma_{e_p}} \right\} \quad (15)$$

$$\mathbf{P}^{(n)} = \left\{ \mathbf{P}_i^{(n)} = 1 - \left(\frac{e_{p_i}}{e_i} \right)^2 \right\} \quad (16)$$

$$\mathbf{Y} = \text{Classify}(\mathbf{Z}^n, \mathbf{P}^n) \quad (17)$$

$$\mathbf{I} = \text{Feature}_{\text{select}}(\mathbf{Y}, \mathbf{G}^{(n)}). \quad (18)$$

First, each community aggregates the information of other communities guided by intercommunity affinity, and the information change is calculated based on (11). Changes in community information will change intercommunity affinity between communities, thereby updating the topology between communities. The change of intercommunity affinity can be calculated from (12).

Then, each node aggregates the feature information of other nodes within the same community, and (13) calculates the information of each node after the k th intracommunity node feature information aggregation process. Changes in node information result in a change in edge weights among nodes within a community, and the topology of the entire BG-N will be updated. An increasingly clear community structure can be detected as a result of the new higher order graph structure information. The process is described by (14).

Ultimately, after n times of affinity aggregation, intracommunity affinity continues to increase, and intercommunity affinity gradually decreases, resulting in a stable community structure. Based on the final BG-CN, (15) and (16) calculate two metrics of community structure, namely the intracommunity z -score Z and the participation coefficient P [34]. Z_i and P_i measure the connectivity of node i to other nodes in the community and connectivity to other communities in the network, respectively. As a result of the community structural metric analysis, (17) and (18) provide the classification of normal controls (NCs) and AD patients, the extraction of lesioned brain regions, and the identification of risk genes, respectively.

C. Com-GC Neural Network

This section designs the Com-GCN based on the affinity aggregation model constructed for BG-CN, and the

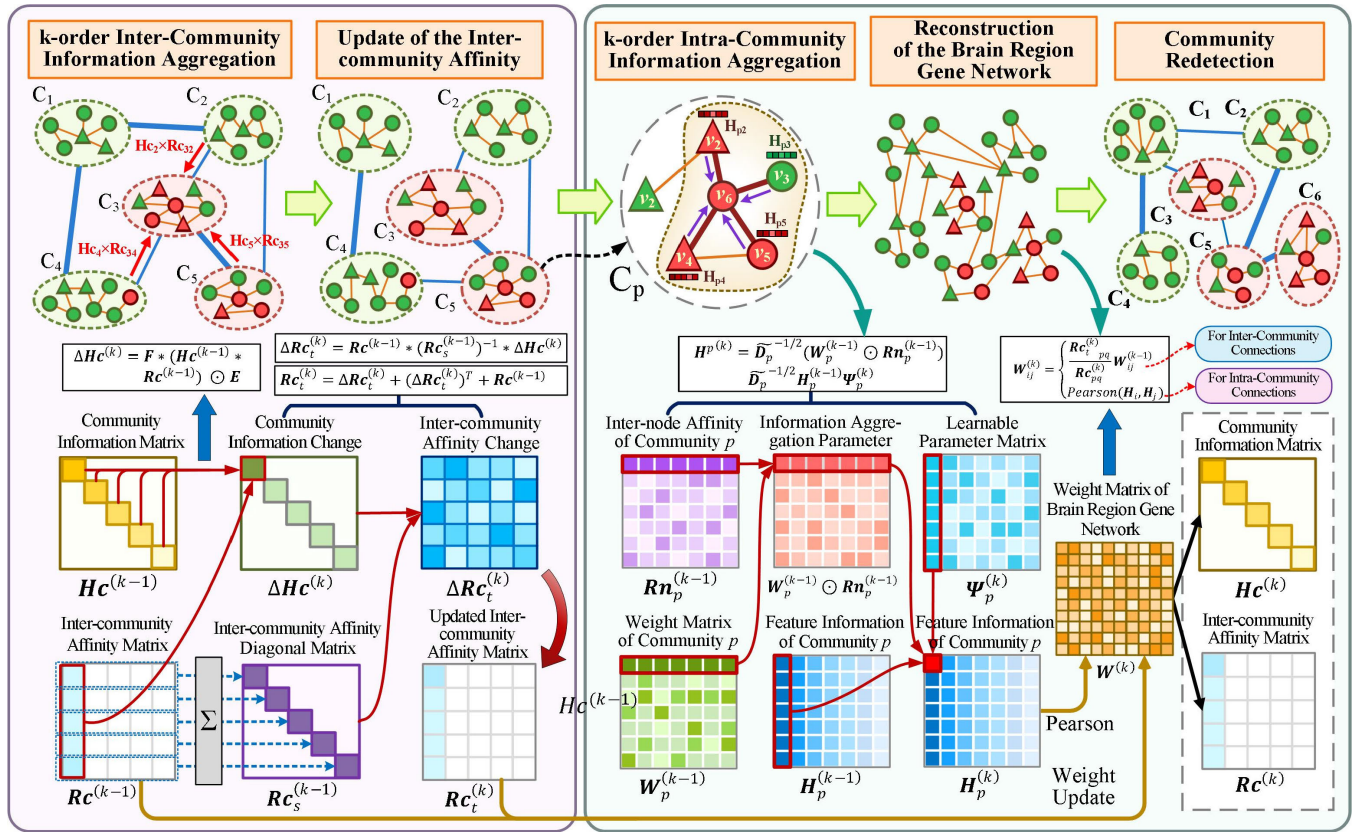


Fig. 2. Process of the designed Com-GC operation.

implementation of Com-GCN uses the Python programming language. Fig. 2 depicts its three components: the input layer, the Com-GC layer, and the fully connected (FC) layer.

Specifically, the community feature matrix $\mathbf{H}^{(k-1)} \in \mathbb{R}^{N \times N}$, the community information matrix $\mathbf{H}\mathbf{c}^{(k-1)} \in \mathbb{R}^{u \times u}$, the inter-community affinity matrix $\mathbf{R}\mathbf{c}^{(k-1)} \in \mathbb{R}^{u \times u}$ and the internode affinity matrix $\mathbf{R}\mathbf{n}_p^{(k-1)}$ within u communities after the $(k-1)$ th affinity aggregation are the inputs. The Com-GC layer consists of multiple Com-GCs, each of which contains two subconvolutions: intercommunity convolution and intracommunity convolution. Essentially, intercommunity convolution is the process by which each community gathers information from neighboring communities so as to update the intercommunity topology. Intracommunity convolution makes each node gather feature information from neighboring nodes within the same community, which updates the topology of the entire BG-N. Based on the community structure and weight matrix obtained from the Com-GC layer, the FC layer calculates the classification results for AD and NC by the SoftMax function with the two community structure feature vectors of each node \mathbf{Z} and \mathbf{P} concatenated as the input. Algorithm 1 describes the entire Com-GCN pipeline.

A more detailed explanation of the Com-GC layer is below, taking the k th affinity aggregation of the BG-CN as an example.

1) *Intercommunity Convolution*: When performing intercommunity convolution, the affinity aggregation is performed based on two matrices, community information matrix $\mathbf{H}\mathbf{c}^{(k-1)}$

Algorithm 1 The Algorithm of Community Graph Convolution Neural Network (Com-GCN)

Input: Node feature information matrix $\mathbf{H}^{(0)} \in \mathbb{R}^{N \times N}$ community information matrix $\mathbf{H}\mathbf{c}^{(0)} \in \mathbb{R}^{u \times u}$, inter-community affinity matrix $\mathbf{R}\mathbf{c}^{(0)} \in \mathbb{R}^{u \times u}$, u inter-node affinity matrices $\mathbf{R}\mathbf{n}_p^{(0)} \in \mathbb{R}^{N_{Cp} \times N_{Cp}}$

Output: The optimal subset of features and the classification results of subjects.

Initialize Iteration number n , weight matrix \mathbf{W}

Repeat:

For $k = 1, \dots, n$ **do**

Calculate $\Delta\mathbf{H}\mathbf{c}^{(k)}$ using $\mathbf{H}\mathbf{c}^{(k-1)}$ and $\mathbf{R}\mathbf{c}^{(k-1)}$ through (19);

Calculate $\mathbf{R}\mathbf{c}_t^{(k)}$ using $\Delta\mathbf{H}\mathbf{c}^{(k)}$ through (20) and (21);

Calculate $\mathbf{H}^{(k)}$ by $\mathbf{H}^{(k-1)}$ and $\mathbf{R}\mathbf{n}_p^{(k-1)}$ through (22);

Update $\mathbf{W}^{(k)}$ using $\mathbf{R}\mathbf{c}_t^{(k)}$ and $\mathbf{H}^{(k)}$ by (23);

end

For $i = 1, \dots, N$ **do**

Calculate \mathbf{z}_i through (15);

Calculate \mathbf{P}_i through (16);

End

Generate classification result \mathbf{Y} using $\mathbf{Z}^{(n)}$ and $\mathbf{P}^{(n)}$ by (25)

Until the convergence is satisfied.

Obtain importance matrices through (29);

Generate the optimal subset of features by solving (18)

and intercommunity affinity matrix $\mathbf{R}\mathbf{c}^{(k-1)}$. After the intercommunity convolution in the $(k-1)$ th affinity aggregation, the k -order BG-CN is obtained, and the community information change matrix $\Delta\mathbf{H}\mathbf{c}^{(k)} \in \mathbb{R}^{u \times u}$ is defined as follows:

$$\Delta\mathbf{H}\mathbf{c}^{(k)} = \mathbf{F} * (\mathbf{H}\mathbf{c}^{(k-1)} * \mathbf{R}\mathbf{c}^{(k-1)}) \odot \mathbf{E} \quad (19)$$

where $\mathbf{F} \in \mathbb{R}^{u \times u}$ denotes a matrix with all values of 1, \odot denotes the Hadamard product, and $\mathbf{E} \in \mathbb{R}^{u \times u}$ is an identity matrix. $\mathbf{F} * (\mathbf{H}\mathbf{c}^{(k-1)} * \mathbf{R}\mathbf{c}^{(k-1)}) \odot \mathbf{E}$ is a diagonal matrix, where the diagonal elements gather the information that each community received from its neighbor communities. Thus, $\Delta\mathbf{H}\mathbf{c}_{pp}^{(k)}$ denotes the amount of community information change of community p .

The association between communities is updated after community information changes. The calculation of the intercommunity affinity change is as below

$$\Delta\mathbf{R}\mathbf{c}_t^{(k)} = \mathbf{R}\mathbf{c}^{(k-1)} * (\mathbf{R}\mathbf{c}_s^{(k-1)})^{-1} * \Delta\mathbf{H}\mathbf{c}^{(k)} \quad (20)$$

$$\mathbf{R}\mathbf{c}_t^{(k)} = \Delta\mathbf{R}\mathbf{c}_t^{(k)} + (\Delta\mathbf{R}\mathbf{c}_t^{(k)})^T + \mathbf{R}\mathbf{c}^{(k-1)} \quad (21)$$

where $\mathbf{R}\mathbf{c}^{(k-1)}$ is the intercommunity affinity matrix, $\mathbf{R}\mathbf{c}_s^{(k-1)} \in \mathbb{R}^{u \times u}$ is the intercommunity affinity diagonal matrix, and $\mathbf{R}\mathbf{c}_{sp}^{(k-1)}$ in the matrix is the sum of affinities of all intercommunity edges connected to the community p . Therefore, $\mathbf{R}\mathbf{c}^{(k-1)} * (\mathbf{R}\mathbf{c}_s^{(k-1)})^{-1}$ represents the ratio of the affinity of each edge connected to a community to the sum of the affinities of all the edges connected to that community. The element $\Delta\mathbf{R}\mathbf{c}_{tpq}^{(k)}$ in matrix $\Delta\mathbf{R}\mathbf{c}_t^{(k)}$ quantifies the influence that the information change of community p has on the affinity of edge e_{pq} . It should be noted that element $(\Delta\mathbf{R}\mathbf{c}_t^{(k)})_{pq}^T$ in matrix $(\Delta\mathbf{R}\mathbf{c}_t^{(k)})^T$ corresponds to element $\Delta\mathbf{R}\mathbf{c}_{tpq}^{(k)}$ in matrix $\Delta\mathbf{R}\mathbf{c}_t^{(k)}$, which represents the extent to which the change in community information of community q affects the affinity of edge e_{pq} . Consequently, $\Delta\mathbf{R}\mathbf{c}_t^{(k)}$ and $(\Delta\mathbf{R}\mathbf{c}_t^{(k)})^T$ are added to obtain the amount of change in intercommunity affinity, and then $\mathbf{R}\mathbf{c}^{(k-1)}$ is added to obtain the updated intercommunity affinity matrix $\mathbf{R}\mathbf{c}_t^{(k)}$.

2) *Intracommunity Convolution*: During intercommunity convolutions, the affinity aggregation is performed based on the u feature information matrix $\mathbf{H}_p^{(k-1)}$ and u internode affinity matrices $\mathbf{R}\mathbf{n}_p^{(k-1)}$ of the u communities. After the intracommunity convolution in the k th affinity aggregation, each node updates its own feature information. The new node feature information matrix $\mathbf{H}^{(k)}$ is composed of the node feature information matrices of the u communities assembled together, where the node feature information matrix of the p th community $\mathbf{H}_p^{(k)} \in \mathbb{R}^{N_{cp} \times N_{cp}}$ is calculated as follows:

$$\mathbf{H}_p^{(k)} = \text{ReLU}\left(\tilde{\mathbf{D}}_p^{-\frac{1}{2}} * (\mathbf{W}_p^{(k-1)} \odot \mathbf{R}\mathbf{n}_p^{(k-1)}) * \tilde{\mathbf{D}}_p^{-\frac{1}{2}} \mathbf{H}_p^{(k-1)} \Psi_p^{(k)}\right) \quad (22)$$

where $\mathbf{W}_p^{(k-1)} \in \mathbb{R}^{N_{cp} \times N_{cp}}$ and $\mathbf{R}\mathbf{n}_p^{(k-1)} \in \mathbb{R}^{N_{cp} \times N_{cp}}$ denote the weight matrix and internode affinity matrix of the p th community, respectively, $\Psi_p^{(k)} \in \mathbb{R}^{N_{cp} \times l}$ denotes the learnable filter with $N_{cp} \times l$ learnable parameters, N_{cp} shows how many nodes the p th community has, and l is the length of the feature sequence. $\tilde{\mathbf{D}}_p \in \mathbb{R}^{N_{cp} \times N_{cp}}$ denotes the node degree matrix of the p th community, which is used for normalization.

3) *Reconstruction of Community Network*: The updated intercommunity affinity matrix $\mathbf{R}\mathbf{c}^{(k)} \in \mathbb{R}^{u \times u}$ and the feature matrix $\mathbf{H}^{(k)} \in \mathbb{R}^{N \times l}$ can be obtained after the above two

steps. Changes in intercommunity affinity affect the degree of association between communities, leading to changes in edge weights between nodes of different communities, and changes in node feature information affect the degree of association between nodes, leading to changes in edge weights between nodes within a community. The final weight matrix of nodes is calculated as follows:

$$\mathbf{W}_{ij}^{(k)} = \begin{cases} \frac{\mathbf{R}\mathbf{c}_{tpq}^{(k)}}{\mathbf{R}\mathbf{c}_{pq}^{(k)}} \mathbf{W}_{ij}^{(k-1)}, & \text{if } i \in C_p, j \in C_q \\ \text{Pearson}(\mathbf{H}_i, \mathbf{H}_j), & \text{if } i \in C_p, j \in C_p. \end{cases} \quad (23)$$

When the weights change, the topology of the BG-N is updated, and therefore, the community structure of the network is altered as well. The updated weight matrix allows the construction of an updated BG-CN in accordance with the method described in Section III-A.

4) *Classification With FC Layer*: A stable BG-CN is obtained after n times of Com-GC. At the same time, the weight matrix $\mathbf{W}^n \in \mathbb{R}^{N \times N}$ corresponding to the community network is also generated. If the number of communities in the network is u , then the affinity matrices $\mathbf{R}\mathbf{n}_1^n \in \mathbb{R}^{C_1 \times C_1}$, $\mathbf{R}\mathbf{n}_2^n \in \mathbb{R}^{C_2 \times C_2}$, ..., $\mathbf{R}\mathbf{n}_u^n \in \mathbb{R}^{C_u \times C_u}$ between the nodes within each community can be derived.

Based on the weight matrix and the affinity matrix, two modular network metrics for the nodes can be calculated: the intracommunity z -score Z_i and the participation coefficient P_i . These two indicators are used as classification features of the FC layer.

More specifically, we combine these two modular network metrics of this node together and obtain a 1-D feature vector $\mathbf{X}^{(0)}$, which is input to the FC layer. The formula can be expressed as follows:

$$\mathbf{X}^{(0)} = \begin{pmatrix} \mathbf{X}_{1,1}^{(n)} \\ \mathbf{X}_{2,1}^{(n)} \\ \dots \\ \mathbf{X}_{N,1}^{(n)} \\ \mathbf{X}_{N+1,1}^{(n)} \\ \dots \\ \mathbf{X}_{2N,1}^{(n)} \end{pmatrix} = \begin{pmatrix} Z_1^{(n)} \\ P_1^{(n)} \\ Z_2^{(n)} \\ P_2^{(n)} \\ \dots \\ Z_N^{(n)} \\ P_N^{(n)} \end{pmatrix}. \quad (24)$$

For FC layers, the last layer uses $\text{Softmax}(\cdot)$ as the activation function and the others use $\text{ReLU}(\cdot)$. The formula is expressed as follows:

$$\mathbf{X}^{(n+1)} = \begin{cases} \text{ReLU}\left(\Theta^{(h)} * \mathbf{X}^{(h)} + \mathbf{b}^{(h)}\right), & \text{if } h \neq L - 1 \\ \text{Softmax}\left(\Theta^{(h)} * \mathbf{X}^{(h)} + \mathbf{b}^{(h)}\right), & \text{if } h = L - 1 \end{cases} \quad (25)$$

where $\Theta^{(h)}$ and $\mathbf{b}^{(h)}$ denote the weight matrix and the bias between layer h and $h + 1$ in the FC layer, respectively; $\mathbf{X}^{(h)}$ and $\mathbf{X}^{(h+1)}$ are the 1-D vectors of layers h and $h + 1$, respectively; L shows how many layers in the FC layer; $\text{ReLU}(\cdot)$ and $\text{Softmax}(\cdot)$ are both activation functions. The input feature vectors are calculated in the FC layer to map the final true or false discriminations.

D. Feature Extraction With Com-GCN

In order to further explore the differences between AD and NC, the feature extraction part of this study is designed with the following specific steps.

First, the accuracy score A^i is calculated from the output of the Softmax(\cdot) layer in the following way:

$$A^i = D_i \times T_i \quad (26)$$

where D_i and T_i are the predicted and true labels of the subject, respectively.

Second, the importance matrix corresponding to the parameter matrix is calculated. The resulting importance matrix will combine the accuracy scores A^i as a prior condition for obtaining the neuron importance score matrix. The above procedure is formulized as

$$I_{i1}^h = \sum_{j=1}^{a_h} \left| \prod_1^h (\Theta^{(h)})_{ij} \right| \quad (27)$$

$$Ic = \sum_{h=1}^L I^h * \frac{\sum_{i=1}^M A_i}{M} \quad (28)$$

where I_{i1}^h is the h th importance matrix, a_h is the number of columns in the h th learnable parameter matrix, and $h = 1, \dots, L$. M is the number of samples, $(\sum_{i=1}^M A_i / M)$ represents the average accuracy score, and each element of Ic represents the importance score of the community structure index, which also represents the importance score of each neuron.

Third, the importance scores of the nodes are derived from the importance scores of the neurons. The importance score I_i for the i th node is calculated as follows:

$$I_i = Ic_{2i-1} + Ic_{2i}, \quad i = 1, 2, \dots, N \quad (29)$$

where Ic_{2i-1} and Ic_{2i} represent the importance score of Z_i and P_i , respectively.

Additionally, we arrange the nodes in order of decreasing importance. The first, second, \dots , and N th nodes in the arrangement are chosen in increments of one to obtain N node subsets.

Finally, the subsets are input to the Com-GCN, and the classification accuracy is recorded. The accuracy is compared to filter out the optimal subset of features, i.e., abnormal brain regions and genes.

IV. EXPERIMENTAL RESULTS

A. Data Acquisition and Preprocessing

In this article, the experimental data are downloaded from the publicly available database of the ADNI. Medical imaging and genetic data from both healthy individuals and patients are included in the ADNI database and have been authorized for research purposes. In order to evaluate the proposed model from various aspects, data of several AD-like diseases were selected, such as early MCI (EMCI) and late MCI (LMCI). The basic information about the data is listed in Table I. To verify that the experimental results were not influenced

TABLE I
BASIC INFORMATION OF THE DATA

Categories	NC	AD	EMCI	LMCI
Amount	237	233	197	203
Gender (F/M)	95/142	82/151	89/108	95/108
Age (Mean \pm SD)	73.03 \pm 6.060	71.55 \pm 5.896	73.43 \pm 5.45	74.83 \pm 7.92

by the gender and age of the subjects, we conducted chi-square tests and two-sample t-tests to detect interference from gender and age, respectively. In the abovementioned statistical tests, the results for the AD and NC groups were 0.274 and 0.007, respectively, the results for the EMCI and LMCI were 0.745 and 0.041, respectively, and the results for LMCI and AD were 0.193 and 0.001, respectively. According to the results, there were no significant differences among the three subgroups, thus ruling out the interference caused by gender and age.

The fMRI data underwent MATLAB-based preprocessing, involving the removal of the initial ten time points to mitigate magnetic field instability and scan time inconsistency, parameter adjustment for uniformity, head motion correction, spatial standardization, and suppression of noise through physiological noise elimination and filtering. Brain regions were divided based on the anatomical automatic labeling. For SNP data, we used Pink and MATLAB to filter SNPs based on sample deletion rate and Hardy Weinberg equilibrium p -value. The eligible 45 genes were coded based on minimal alleles. Finally, as the approach we proposed, both gene sequences and time sequences were standardized to a length of 70 for ease of filtering. Lengths that were too short filtered out too many genes, while lengths that were too long limited discriminative ability and made analysis challenging. Through repeated experiments, we determined this threshold to ensure feature distinction while expanding the number of genes.

B. Experimental Settings

Considering the comprehensiveness of the comparison experiment, the comparison method of the experiment was selected for global and local comparisons. Specifically, for global comparisons, we selected SVM from traditional machine learning methods and selected DNN, CNN, and GCN as the classical deep learning methods.

On the other hand, local comparisons are conducted between the proposed method and its variants. We removed the intercommunity convolution and intracommunity convolution of Com-GCN, respectively, resulting in two variants of Com-GCN (without Intercom) and Com-GCN (without Intracom). These two variants of the proposed method were selected as two additional comparison methods. In addition, ACC, sensitivity (SEN), specificity (SPE), and the area under the curve (AUC) were chosen as evaluation indicators for experiments. Furthermore, the experiments are divided into three

TABLE II
COMPARISON OF CLASSIFICATION PERFORMANCE

Method	NC vs. AD				EMCI vs. LMCI				LMCI vs. AD			
	ACC(%)	SPE(%)	SEN(%)	AUC(%)	ACC(%)	SPE(%)	SEN(%)	AUC(%)	ACC(%)	SPE(%)	SEN(%)	AUC(%)
SVM	67.02	71.05	64.28	68.56	66.25	67.30	64.28	66.75	66.67	68.42	65.30	67.81
DNN	71.28	69.04	73.07	73.24	70.00	71.42	67.74	73.16	71.26	70.00	72.97	72.84
CNN	74.47	76.08	72.91	75.89	72.50	70.83	75.00	74.68	73.56	72.00	75.67	75.31
GCN	79.79	81.57	78.57	80.48	77.50	78.26	76.47	79.35	78.16	76.47	79.24	78.52
Com-GCN (without Intra-Com)	85.10	86.11	84.48	86.95	83.75	88.89	82.25	84.85	83.91	86.20	82.75	85.69
Com-GCN (without Inter-Com)	87.23	84.61	87.65	89.16	85.00	86.67	84.51	87.73	86.21	84.61	86.48	88.26
Com-GCN	93.61	92.10	94.54	95.12	90.00	92.10	88.09	93.22	91.95	90.90	92.59	92.86

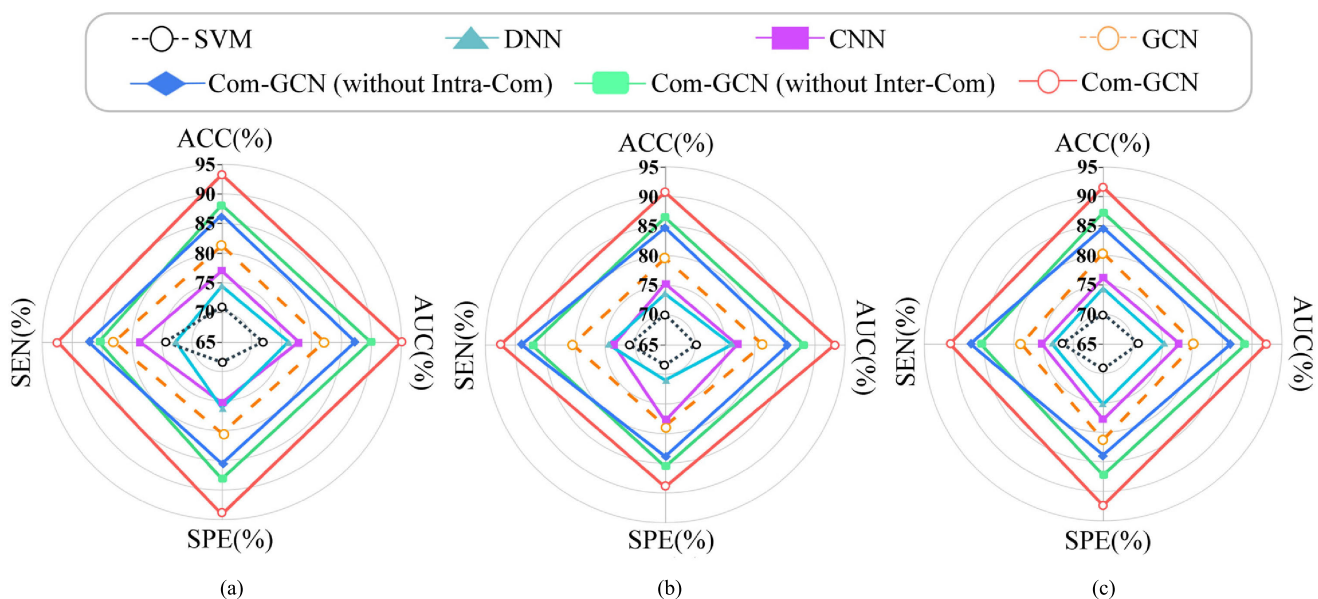


Fig. 3. Performance comparison in tasks (a) NC versus AD, (b) EMCI versus LMCI, and (c) LMCI versus AD.

classification tasks: AD versus NC, EMCI versus LMCI, and LMCI versus AD.

C. Performance Comparison

Table II presents the classification results. In addition, the radar charts in Fig. 3 show the results of the performance comparison. As shown, Com-GCN outperformed other methods in all four metrics for three classification tasks. In particular, in the classification task of AD and NC, our method achieves an accuracy of 93.61%. The results proved the successful application of Com-GC in imaging genetics. Moreover, the advantages of graph convolution were demonstrated in this experiment. Deep learning methods based on graph convolution always outperform traditional machine learning methods. Finally, the performance of the two variants is inferior to the proposed method, and the effectiveness of the Com-GC has also been proven.

D. Results of Model Adjustment

This section tested the correlation between classification performance and the methods for constructing BG-N. Fig. 4 displays the comparison results by histograms. The results show that using the PC to construct BG-N can significantly improve the performance.

For further exploration, the proportion of intercommunity information aggregation α and the proportion of intracommunity information aggregation β need to be optimized. We found the best combination of the two parameters by increasing α and β from 0 to 1 and recording the changes of classification accuracy. Fig. 5 shows all results. Com-GCN achieved the highest accuracy when $\alpha = 0.8$ and $\beta = 0.9$.

E. Effects of Com-GC on Feature Extraction

Accurately identifying the affected brain regions and high-risk genes is of paramount importance. This section

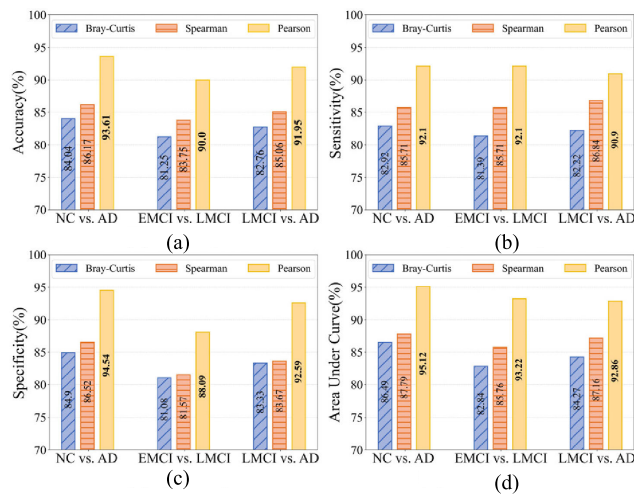


Fig. 4. Performance comparison among methods in indexes of (a) accuracy, (b) sensitivity, (c) specificity, and (d) area under the curve.

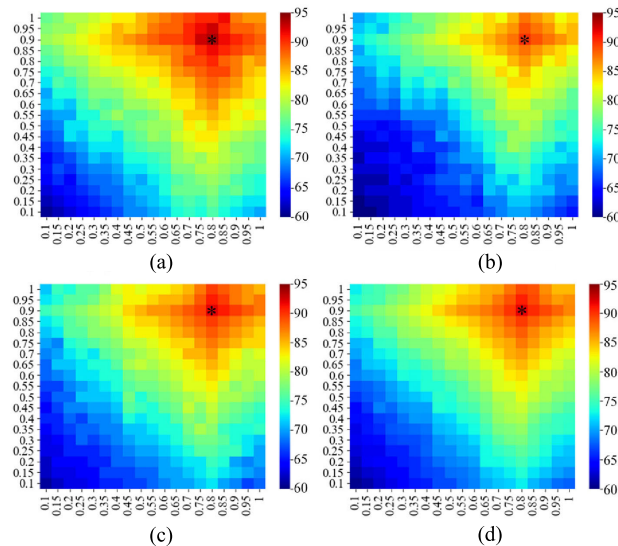


Fig. 5. Results of parameter optimization in three different classification tasks. (a) NC versus AD, (b) EMCI versus LMCI, (c) LMCI versus AD, and (d) average results.

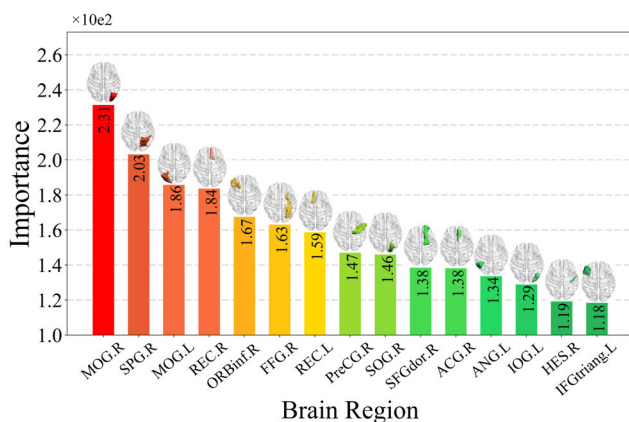


Fig. 6. First 15 brain regions with the highest scores extracted by Com-GCN.

showed the pathogenic factors extracted by the Com-GCN ranked in order of importance in Figs. 6 and 7. The visualization of the brain in Fig. 6 is drawn by the BrainNet

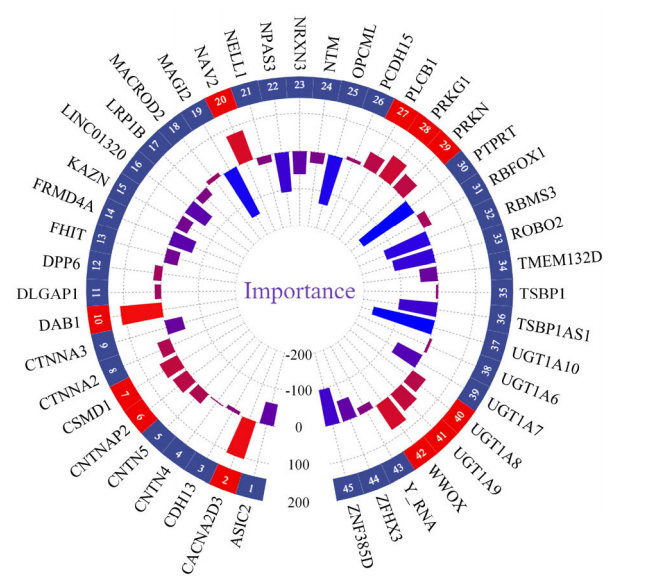


Fig. 7. Importance scores for genes extracted by Com-GCN.

Viewer tool in MATLAB software. It can be observed that the key risk features identified in this study are MOG.R, REC.R, FFG.R, and IFGtriang.L for brain regions and NAV2, WWOX, and DAB1 for genes, which were also confirmed in previous studies. For example, Palejwala et al. [35] found that the information transfer of recognition and perception mostly relies on MOG.R, SOG.R. Lei et al. [36] proposed a new model that enabled identification and feature extraction of early stages of AD, and their results showed that REC.R and SOG.R, etc. are the key brain regions for identifying AD. Zhao et al. [37] proposed new representations and applied them to whole brain signals to identify affected diseased brain regions, and the experimental results showed that the functional connectivity of some brain regions, such as FFG.R, was reduced. IFGtriang.L is found to have an important connection with visual creativity and recognition of the brain [38]. Wang et al. [39] identified several genetic variants within the NAV2 gene that affected AD risk in their study. Dugan et al. [40] show that the WWOX locus has been identified as potential AD risk variants.

To further confirm the discriminating abilities of the features, t-tests were used to test the features extracted by all methods, i.e., the extracted brain regions and genes. Fig. 8 shows that most p -values of features extracted by Com-GCN are less than 0.05. The comparison methods generally had higher p -values and extracted far more features than the target method.

In addition, we combined the extracted discriminative brain regions and genes one by one, calculated the association between these brain region-gene combinations using PC coefficients, and calculated the significant differences between NC and AD for these combinations using standard t-tests. The results show that the p -values for most of the combinations are less than 0.05. These combinations are marked with an asterisk in Fig. 9. This also illustrates the effectiveness of our method in feature extraction from another perspective.

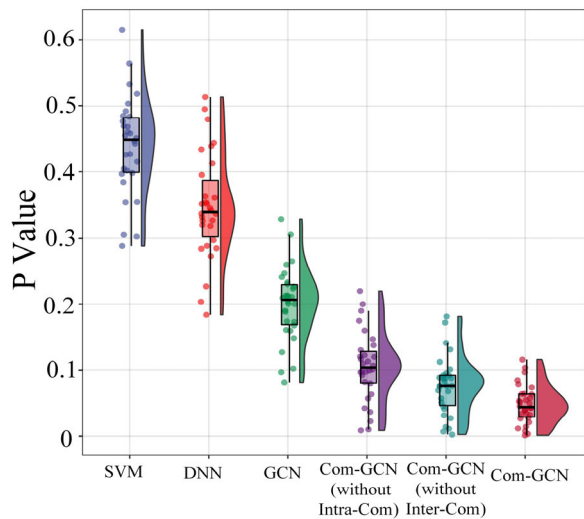


Fig. 8. p -value distribution results by extracted features.

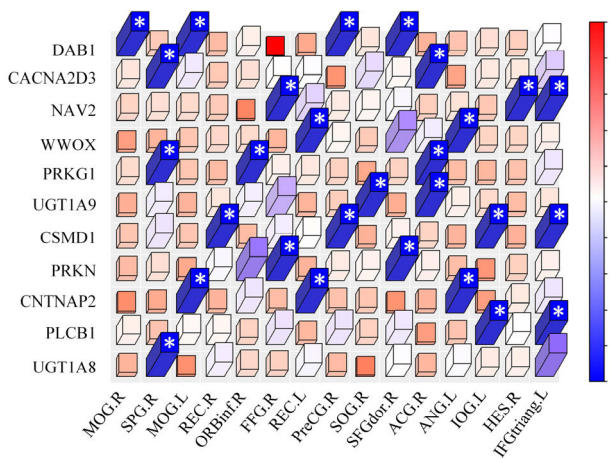


Fig. 9. p -values of the brain region-gene combinations. The asterisks indicate p -values that are lower than 0.05.

Summarizing the above, Com-GCN automatically selected the most scientifically valuable and easily distinguishable features, which possess strong classification power for NC and AD. These features reveal pronounced differences between NC and AD, indicating that the brain regions and genes within them are more susceptible to functional or structural damage and abnormal expression. In addition, Com-GCN suggests potential directions for future research by identifying brain regions or genes that have not been established as linked to AD. These features can provide clinicians with valuable insights to better understand their role and rationality in relation to the disease.

F. Comparison Results With State-of-Art Methods

In this section, traditional machine learning methods [41], [42] and deep learning methods [43], [44] published in recent years are selected as comparison methods to verify the progressiveness of the Com-GCN. It can be observed from Table III that our method performs the best, which also shows

TABLE III
COMPARISON RESULTS WITH STATE-OF-ART METHODS

Methods	Data	ACC
Dadi et al., 2019	402 ASD vs. 464 NC	69.70%
	40 AD vs. 96 MCI	72.20%
Jiang et al., 2020	402 ASD vs. 466 NC	73.10%
	34 AD vs. 99 MCI	78.50%
Hao et al., 2020	44 EMCI vs. 38 LMCI	84.47%
Li et al., 2019	194 AD vs. 216 NC	89.10%
	164 pMCI vs. 233 sMCI	72.50%
Peng et al., 2019	93 MCI vs. 47 NC	80.30%
	49 AD vs. 93 MCI	76.90%
Proposed method	197 EMCI vs. 203 LMCI	90.00%
	203 LMCI vs. 233 AD	91.95%
	237 NC vs. 233 AD	93.61%

that the combination of community and graph convolution is of great effectiveness in imaging genetics analysis.

V. DISCUSSION

A. Effectiveness of the Com-GC

To verify the effectiveness of Com-GC, three features were randomly selected among the extracted distinguishing features, and the three features numbered 4, 27, and 32, respectively, and the impact of Com-GC on the community structure with these features under the three classification tasks was visualized. First, for each subject, two community structure metrics Z_i and P_i of distinguishing features based on the initial BG-CN are calculated. Second, two metrics were calculated based on the finalized BG-CN after n times of Com-GC operations. Finally, the corresponding values were visualized according to subject categories. The effect of Com-GC on the community structure is visualized in Fig. 10; after Com-GC, most noise of the features is suppressed, and the differentiation across disease states is pronounced. This explains the superiority of Com-GC in classification accuracy.

In addition, the t-distributed stochastic neighbor embedding (t-SNE) method was used to visualize the effect of Com-GC on the weight matrix. Based on the three classification tasks, the overall cluster comparison was divided into three parts: the original weight matrix, the weight matrix after GCN convolution, and the weight matrix after Com-GCN. The results shown in Fig. 11 demonstrate that the Com-GC makes a better clustering of the original weight matrices in all three classification tasks.

Furthermore, the community structures of NC and AD divided by Com-GC are also visualized. We averaged the BG-Ns of all NC and AD subjects to obtain two groups of average BG-Ns. Then, according to the construction of BG-CN, the community detection of the average BG-N of the AD group and the NC group is completed. As a result, the average BG-CNs of the two groups were obtained, with edge weights below the threshold set to 0 for a clearer presentation

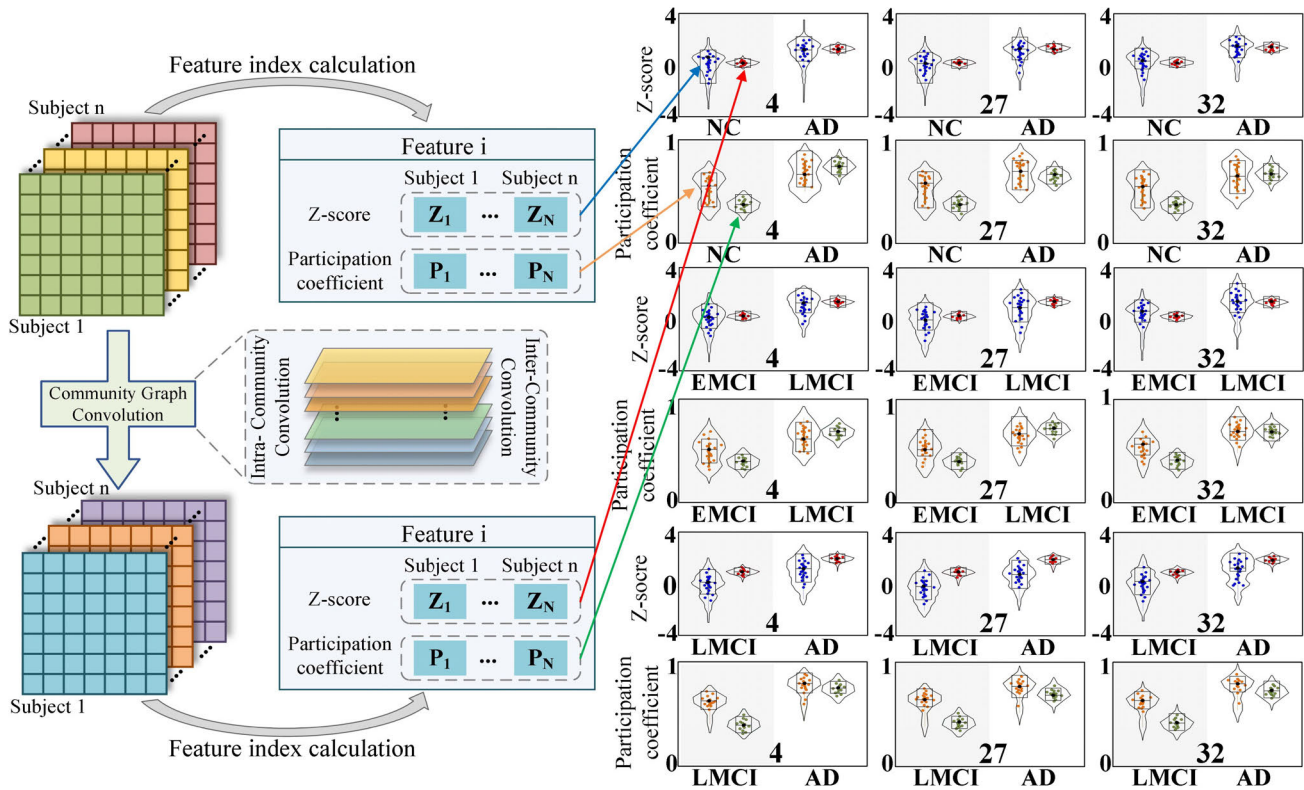


Fig. 10. Procedures to verify the effectiveness of the proposed convolution operations.

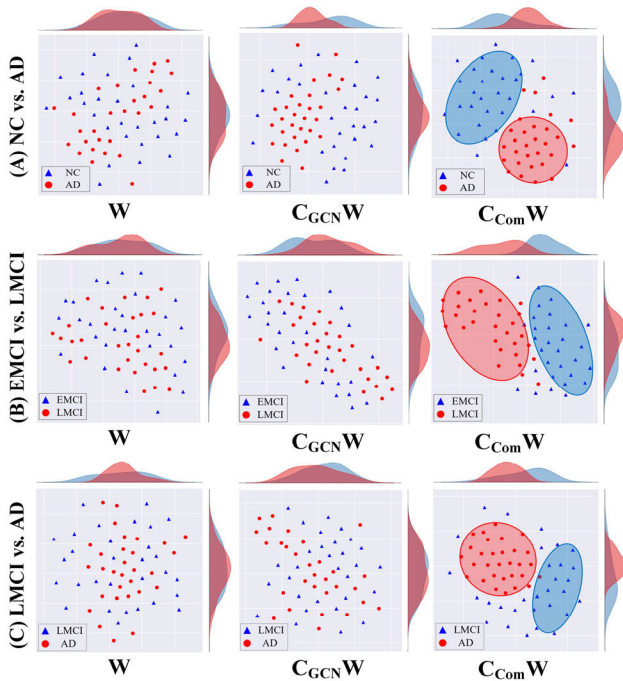


Fig. 11. Effects of Com-GC on clustering.

of feature association patterns for both disease development stages. Fig. 12 displays community division results and intercommunity connections, while Fig. 13 shows intercommunity connections. Several conclusions can be drawn from the figures. First, the community number of AD is generally more than that of NC. In AD development, some functional

connections among AD patients have been hampered, and the connections within the community have been broken, resulting in the division of communities [45]. Second, the community sizes in the AD group differ greatly from each other. Physiological research shows that when the diseased brain regions attempt to complete physiological activities, compensation will occur in other brain regions or genes, which is also well reflected in changes in the community size. Finally, the community connections of the AD group are more scattered than those of the NC group, which also reflects the disconnection between brain regions and genes due to pathological changes.

B. Comparison of Model Training

Fig. 14 describes the loss curves and convergence curves for each method. Although the GCN and the two variants had stabilized by the end of the training, they had higher losses than the Com-GCN. Also, the proposed method is the first to converge and achieves the highest accuracy after convergence. This also proves that the proposed method has better generalization and robustness.

C. Limitations and Future Work

This article designs detailed convolution operations based on the community structure and incorporates brain imaging data on the community structure and incorporates brain imaging data into the model. Results validate the potential of our method, but our works are currently limited by the environment and hardware configuration. At present, the study is conducted only at the level of brain regions and

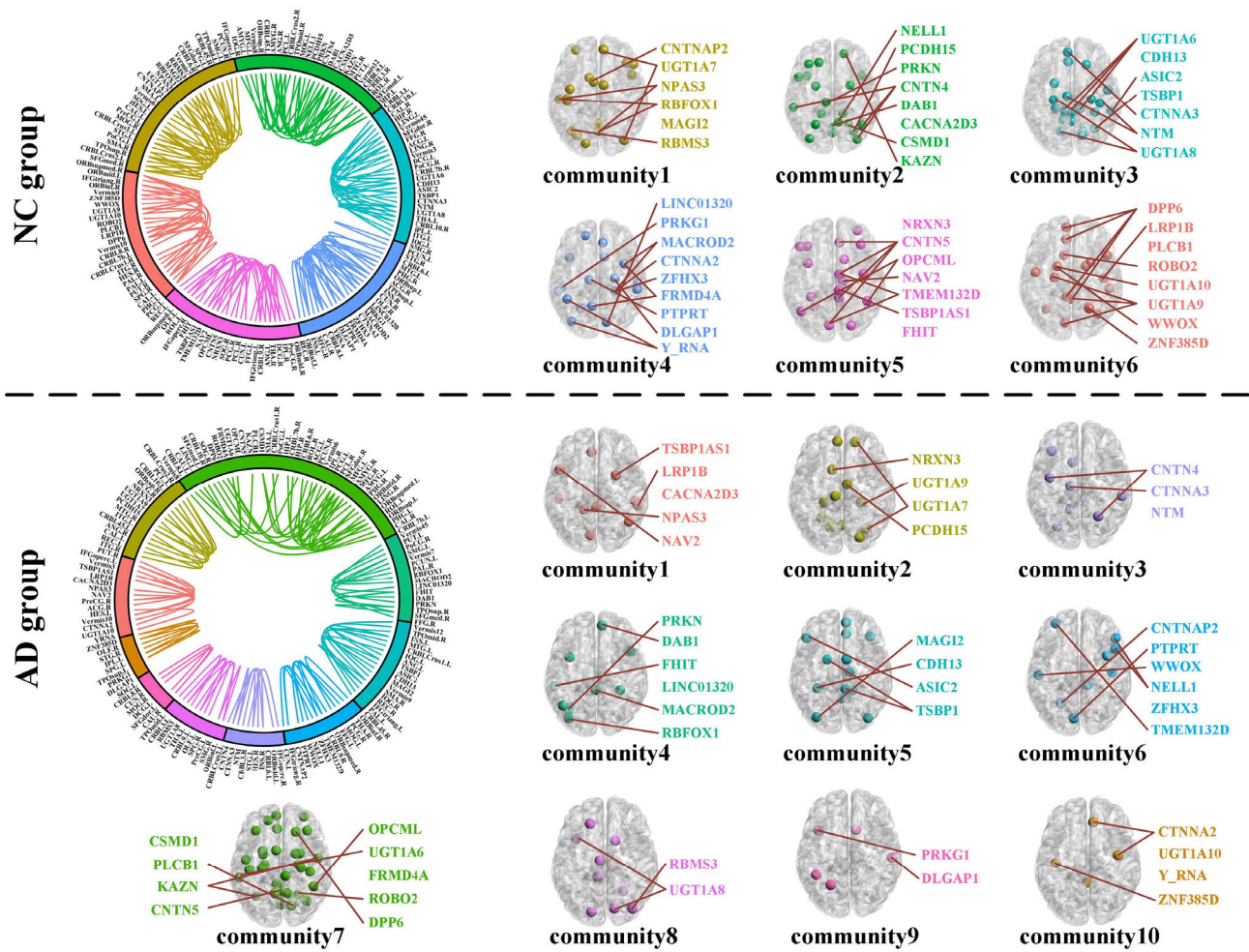


Fig. 12. Results of NC and AD group divisions within the community.

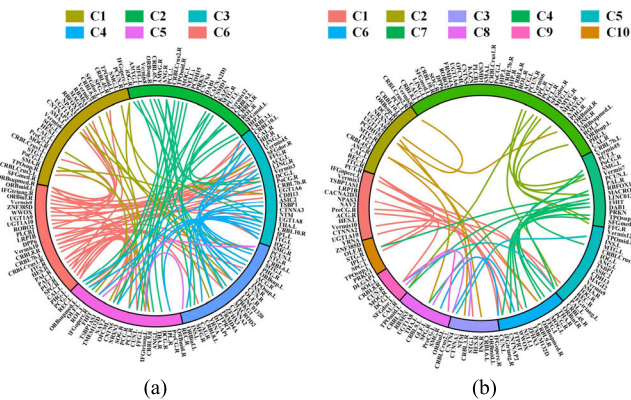


Fig. 13. Results of NC and AD group divisions among the community. (a) NC. (b) AD.

genes. Better computational resources will empower us to study brain community activities at the mesoscopic neuronal population level. In that case, we can better understand the cognitive functions of the brain and develop deeper neural networks and brain-like computing. To simulate community activities and mechanisms of the brain at macro-medium-micro scales, we propose the “Manhattan Project for Brain-like

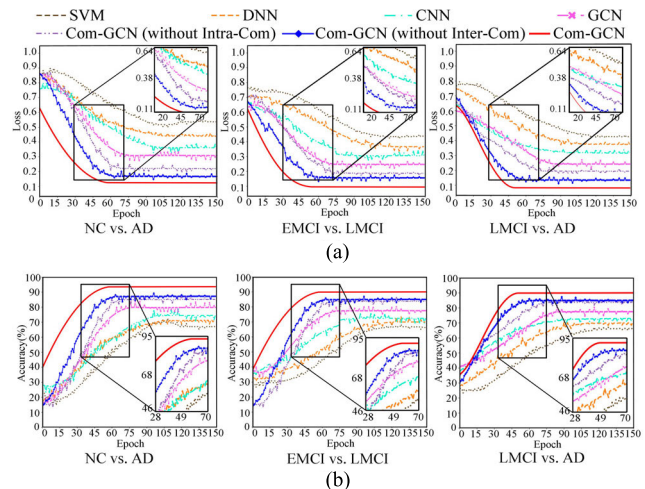


Fig. 14. Comparison between different methods in (a) loss curves and (b) convergence curves.

Neural Networks” for the brain and hope that the government and academia will support this endeavor in the future. In this way, the data can be scaled up in the future, and methods such as transfer learning can be considered to integrate more diverse biomedical data from other datasets into our study.

VI. CONCLUSION

This article proposes Com-GCN, a method that incorporates community theory and deep learning to diagnose AD and automatically identify risk genes and diseased brain regions. Specifically, BG-CNs are constructed based on brain imaging genetics data of AD patients and NC, and the intracommunity and intercommunity information interaction is modeled by the affinity aggregation model. Furthermore, the intercommunity and intracommunity convolution operations in the Com-GC layer are designed to allow the method to extract salient regions that are advantageous for classification during the training process, thus improving its classification performance. Finally, the differences in community structure between the two disease states are fully explored in order to identify the causal factors. Experiments on subjects from ADNI demonstrate the effectiveness of Com-GCN in AD diagnosis and causative factor extraction tasks. Additionally, Com-GCN has greater interpretability than other deep learning methods. Our design of Com-GC is consistent with actual physiological mechanisms, which makes it a valuable reference when studying brain disorders other than AD.

REFERENCES

- [1] C. Lian, M. Liu, J. Zhang, and D. Shen, "Hierarchical fully convolutional network for joint atrophy localization and Alzheimer's disease diagnosis using structural MRI," *IEEE Trans. Pattern Anal. Mach. Intell.*, vol. 42, no. 4, pp. 880–893, Apr. 2020.
- [2] X. Song et al., "Graph convolution network with similarity awareness and adaptive calibration for disease-induced deterioration prediction," *Med. Image Anal.*, vol. 69, Apr. 2021, Art. no. 101947.
- [3] L. Wang, L. Wong, Z.-H. You, D.-S. Huang, X.-R. Su, and B.-W. Zhao, "NSECDA: Natural semantic enhancement for CircRNA-disease association prediction," *IEEE J. Biomed. Health Informat.*, vol. 26, no. 10, pp. 5075–5084, Oct. 2022.
- [4] G. Novikova et al., "Integration of Alzheimer's disease genetics and myeloid genomics identifies disease risk regulatory elements and genes," *Nature Commun.*, vol. 12, no. 1, pp. 1–14, Mar. 2021.
- [5] C. Lian, M. Liu, L. Wang, and D. Shen, "Multi-task weakly-supervised attention network for dementia status estimation with structural MRI," *IEEE Trans. Neural Netw. Learn. Syst.*, vol. 33, no. 8, pp. 4056–4068, Aug. 2022.
- [6] A. S. L. Ng et al., "Distinct network topology in Alzheimer's disease and behavioral variant frontotemporal dementia," *Alzheimer's Res. Therapy*, vol. 13, no. 1, pp. 1–16, 2021.
- [7] M. M. Sperry, S. Kartha, E. J. Granquist, and B. A. Winkelstein, "Inter-subject FDG PET brain networks exhibit multi-scale community structure with different normalization techniques," *Ann. Biomed. Eng.*, vol. 46, no. 7, pp. 1001–1012, Jul. 2018.
- [8] R. Shang, W. Zhang, L. Jiao, X. Zhang, and R. Stolkin, "Dynamic immunization node model for complex networks based on community structure and threshold," *IEEE Trans. Cybern.*, vol. 52, no. 3, pp. 1539–1552, Mar. 2022.
- [9] Z. Duan, X. Sun, S. Zhao, J. Chen, Y. Zhang, and J. Tang, "Hierarchical community structure preserving approach for network embedding," *Inf. Sci.*, vol. 546, pp. 1084–1096, Feb. 2021.
- [10] T. Wen and K. H. Cheong, "The fractal dimension of complex networks: A review," *Inf. Fusion*, vol. 73, pp. 87–102, Sep. 2021.
- [11] Q. Zou, Y. Li, X. Yang, and Z. Zhou, "Identification of key nodes in directed network based on overlapping community structure," *Autom. Control Comput. Sci.*, vol. 55, no. 2, pp. 167–176, Mar. 2021.
- [12] A. Ghasemian, H. Hosseinmardi, A. Galstyan, E. M. Airoidi, and A. Clauset, "Stacking models for nearly optimal link prediction in complex networks," *Proc. Nat. Acad. Sci. USA*, vol. 117, no. 38, pp. 23393–23400, Sep. 2020.
- [13] A. Rossi, D. Barbosa, D. Firmani, A. Matinata, and P. Merialdo, "Knowledge graph embedding for link prediction: A comparative analysis," *ACM Trans. Knowl. Discovery Data*, vol. 15, no. 2, pp. 1–49, 2021.
- [14] I. Rivalta and V. S. Batista, "Community network analysis of allosteric proteins," in *Allostery*, vol. 2253. New York, NY, USA: Springer, 2021, pp. 137–151.
- [15] A. Saltalamacchia, L. Casalino, J. Borišek, V. S. Batista, I. Rivalta, and A. Magistrato, "Decrypting the information exchange pathways across the spliceosome machinery," *J. Amer. Chem. Soc.*, vol. 142, no. 18, pp. 8403–8411, May 2020.
- [16] D. Jin, R. Li, and J. Xu, "Multiscale community detection in functional brain networks constructed using dynamic time warping," *IEEE Trans. Neural Syst. Rehabil. Eng.*, vol. 28, no. 1, pp. 52–61, Jan. 2020.
- [17] J. A. Contreras et al., "Resting state network modularity along the prodromal late onset Alzheimer's disease continuum," *NeuroImage, Clin.*, vol. 22, Jan. 2019, Art. no. 101687.
- [18] S. I. Dimitriadis, E. Messaritaki, and D. Jones, "The impact of graph construction scheme and community detection algorithm on the repeatability of community and hub identification in structural brain networks," *Hum. Brain Mapping*, vol. 42, no. 13, pp. 4261–4280, Sep. 2021.
- [19] C.-M. Ting, S. B. Samdin, M. Tang, and H. Ombao, "Detecting dynamic community structure in functional brain networks across individuals: A multilayer approach," *IEEE Trans. Med. Imag.*, vol. 40, no. 2, pp. 468–480, Feb. 2021.
- [20] L. Du et al., "Associating multi-modal brain imaging phenotypes and genetic risk factors via a dirty multi-task learning method," *IEEE Trans. Med. Imag.*, vol. 39, no. 11, pp. 3416–3428, Nov. 2020.
- [21] L. Du et al., "Identifying progressive imaging genetic patterns via multi-task sparse canonical correlation analysis: A longitudinal study of the ADNI cohort," *Bioinformatics*, vol. 35, no. 14, pp. i474–i483, Jul. 2019.
- [22] X. Hao et al., "Mining outcome-relevant brain imaging genetic associations via three-way sparse canonical correlation analysis in Alzheimer's disease," *Sci. Rep.*, vol. 7, no. 1, pp. 1–12, 2017.
- [23] H.-C. Yi, Z.-H. You, D.-S. Huang, and C. K. Kwok, "Graph representation learning in bioinformatics: Trends, methods and applications," *Briefings Bioinf.*, vol. 23, no. 1, Jan. 2022, Art. no. bbab340.
- [24] J. Jin et al., "IDNA-ABF: Multi-scale deep biological language learning model for the interpretable prediction of DNA methylations," *Genome Biol.*, vol. 23, no. 1, pp. 1–23, Oct. 2022.
- [25] Q. Su, F. Wang, D. Chen, G. Chen, C. Li, and L. Wei, "Deep convolutional neural networks with ensemble learning and transfer learning for automated detection of gastrointestinal diseases," *Comput. Biol. Med.*, vol. 150, Nov. 2022, Art. no. 106054.
- [26] D. Jin et al., "Grab-AD: Generalizability and reproducibility of altered brain activity and diagnostic classification in Alzheimer's disease," *Hum. Brain Mapping*, vol. 41, no. 12, pp. 3379–3391, Aug. 2020.
- [27] S. Basheera and M. S. S. Ram, "A novel CNN based Alzheimer's disease classification using hybrid enhanced ICA segmented gray matter of MRI," *Comput. Med. Imag. Graph.*, vol. 81, Apr. 2020, Art. no. 101713.
- [28] Y. Li et al., "Brain connectivity based graph convolutional networks and its application to infant age prediction," *IEEE Trans. Med. Imag.*, vol. 41, no. 10, pp. 2764–2776, Oct. 2022.
- [29] H.-Y. Zhang et al., "iGRLCDA: Identifying circRNA–disease association based on graph representation learning," *Briefings Bioinf.*, vol. 23, no. 3, May 2022, Art. no. bbac083.
- [30] L. Wang et al., "A machine learning framework based on multi-source feature fusion for circRNA-disease association prediction," *Briefings Bioinf.*, vol. 23, no. 5, Sep. 2022, Art. no. bbac388.
- [31] Y. Zhu, J. Ma, C. Yuan, and X. Zhu, "Interpretable learning based dynamic graph convolutional networks for Alzheimer's disease analysis," *Inf. Fusion*, vol. 77, pp. 53–61, Jan. 2022.
- [32] M. E. J. Newman, "Modularity and community structure in networks," *Proc. Nat. Acad. Sci. USA*, vol. 103, no. 23, pp. 8577–8582, Jun. 2006.
- [33] J. Lee, S. P. Gross, and J. Lee, "Modularity optimization by conformational space annealing," *Phys. Rev. E, Stat. Phys. Plasmas Fluids Relat. Interdiscip. Top.*, vol. 85, no. 5, May 2012, Art. no. 056702.
- [34] R. Guimerà and L. A. N. Amaral, "Functional cartography of complex metabolic networks," *Nature*, vol. 433, no. 7028, pp. 895–900, Feb. 2005.
- [35] A. H. Palejwala et al., "Anatomy and white matter connections of the lateral occipital cortex," *Surgical Radiol. Anatomy*, vol. 42, no. 3, pp. 315–328, Mar. 2020.
- [36] B. Lei et al., "Self-calibrated brain network estimation and joint non-convex multi-task learning for identification of early Alzheimer's disease," *Med. Image Anal.*, vol. 61, Apr. 2020, Art. no. 101652.

- [37] Q. Zhao, H. Lu, H. Metmer, W. X. Y. Li, and J. Lu, "Evaluating functional connectivity of executive control network and frontoparietal network in Alzheimer's disease," *Brain Res.*, vol. 1678, pp. 262–272, Jan. 2018.
- [38] Y. Cai et al., "Relation of visual creative imagery manipulation to resting-state brain oscillations," *Brain Imag. Behav.*, vol. 12, no. 1, pp. 258–273, Feb. 2018.
- [39] K.-S. Wang, Y. Liu, C. Xu, X. Liu, and X. Luo, "Family-based association analysis of NAV2 gene with the risk and age at onset of Alzheimer's disease," *J. Neuroimmunol.*, vol. 310, pp. 60–65, Sep. 2017.
- [40] A. J. Dugan et al., "Association between WWOX/MAF variants and dementia-related neuropathologic endophenotypes," *Neurobiol. Aging*, vol. 111, pp. 95–106, Mar. 2022.
- [41] J. Peng, X. Zhu, Y. Wang, L. An, and D. Shen, "Structured sparsity regularized multiple kernel learning for Alzheimer's disease diagnosis," *Pattern Recognit.*, vol. 88, pp. 370–382, Apr. 2019.
- [42] X. Hao et al., "Multi-modal neuroimaging feature selection with consistent metric constraint for diagnosis of Alzheimer's disease," *Med. Image Anal.*, vol. 60, Feb. 2020, Art. no. 101625.
- [43] K. Dadi et al., "Benchmarking functional connectome-based predictive models for resting-state fMRI," *NeuroImage*, vol. 192, pp. 115–134, May 2019.
- [44] F. Li and M. Liu, "A hybrid convolutional and recurrent neural network for hippocampus analysis in Alzheimer's disease," *J. Neurosci. Methods*, vol. 323, pp. 108–118, Jul. 2019.
- [45] Z. Dai et al., "Disrupted structural and functional brain networks in Alzheimer's disease," *Neurobiol. Aging*, vol. 75, pp. 71–82, Mar. 2019.



Xia-An Bi (Member, IEEE) received the Ph.D. degree in computer applications from Hunan University, Changsha, China, in 2012.

He is currently a Professor with the College of Information Science and Engineering, Hunan Normal University, Changsha. He is the author or coauthor of several technical papers, including several ESI Highly Cited Papers according to the most recent Clarivate Analytics ESI report, and also a very active reviewer for many international journals and conferences. His current research interests include

machine learning, brain science, and artificial intelligence.

Dr. Bi is a member of MICCAI and CCF.



Ke Chen received the B.E. degree in Internet of Things Engineering from Anhui Polytechnic University, Wuhu, China, in 2021. He is currently pursuing the M.S. degree in computer technology with the College of Information Science and Engineering, Hunan Normal University, Changsha, China.

His main research fields include data mining, brain science, and artificial intelligence.



Siyu Jiang received the B.E. degree in Internet of Things Engineering from Anhui Normal University, Wuhu, China, in 2022. He is currently pursuing the M.S. degree in computer technology with the College of Information Science and Engineering, Hunan Normal University, Changsha, China.

His main research fields include data mining, brain science, and artificial intelligence.



Sheng Luo received the B.E. degree in computer science and technology from the Hunan University of Science and Technology, Xiangtan, China, in 2020. He is currently pursuing the M.S. degree in computer technology with the College of Information Science and Engineering, Hunan Normal University, Changsha, China.

His main research fields include data mining, brain science, and artificial intelligence.



Wenyan Zhou received the B.E. degree in computer science and technology from Jinggangshan University, Ji'an, China, in 2020. She is currently pursuing the M.S. degree in computer technology with the College of Information Science and Engineering, Hunan Normal University, Changsha, China.

Her main research fields include data mining, brain science, and artificial intelligence.



Zhaoxu Xing received the B.E. degree in computer science and technology from Hunan Normal University, Changsha, China, in 2019, where he is currently pursuing the M.S. degree in computer science and technology with the College of Information Science and Engineering.

His main research fields include data mining, brain science, and artificial intelligence.



Luyun Xu received the Ph.D. degree in business administration from Hunan University, Changsha, China, in 2018.

She is currently an Associate Professor with the Business School, Hunan Normal University, Changsha. Her research interests focus on knowledge management, data mining, machine learning, and brain science. She has published in *The Journal of Technology Transfer*, *Technology Analysis and Strategic Management*, *Computational and Mathematical Organization Theory*, and *Briefings in Bioinformatics*.



Zhengliang Liu received the B.A. and M.S. degrees in computer science from the University of Wisconsin–Madison, Madison, WI, USA, and Washington University in St. Louis, St. Louis, MO, USA, in 2018 and 2021, respectively. He is currently pursuing the Ph.D. degree with the School of Computing, University of Georgia, Athens, GA, USA.

His main research fields include biomedical natural language processing, biomedical image analysis, and the intersection of machine learning and radiation oncology.



Tianming Liu (Senior Member, IEEE) serves as the Director of the Center for Brain-Inspired Artificial Intelligence and is also a Distinguished Research Professor of Computer Science at the University of Georgia, Athens, GA, USA. In the past two decades, his research has focused on brain imaging, computational neuroscience, and brain-inspired artificial intelligence. He has published over 400 peer-reviewed manuscripts on these topics with H-index 54.

Dr. Liu is a fellow of the American Institute for Medical and Biological Engineering (AIMBE). He received the prestigious NSF CAREER Award and NIH Career Award for his pioneering research works. He was the General Chair of the Medical Image Computing and Computer-Assisted Interventions (MICCAI) in 2019. He serves on the editorial boards of multiple prestigious international journals, including *Medical Image Analysis*, *IEEE TRANSACTIONS ON MEDICAL IMAGING*, *IEEE REVIEWS IN BIOMEDICAL ENGINEERING*, *IEEE/ACM TRANSACTIONS ON COMPUTATIONAL BIOLOGY AND BIOINFORMATICS*, and *IEEE JOURNAL OF BIOMEDICAL AND HEALTH INFORMATICS*.